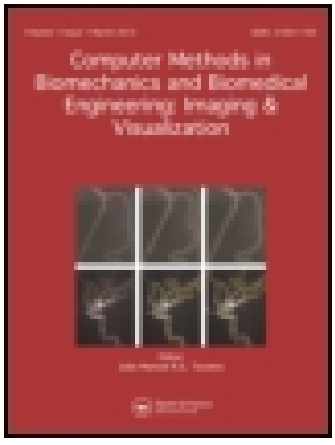

Computer Methods in Biomechanics and Biomedical Engineering: Imaging & Visualization
Publication details, including instructions for authors and subscription information:
http://www.tandfonline.com/loi/tciv20

A system for the detection of melanomas in dermoscopy images using shape and symmetry features

Margarida Ruela[a], Catarina Barata[a], Jorge S. Marques[a] & Jorge Rozeira[b]
[a] Institute for Systems and Robotics, Instituto Superior Técnico, Lisboa, Portugal
[b] Hospital Pedro Hispano, Matosinhos, Portugal
Published online: 12 May 2015.

Computer Methods in Biomechanics and Biomedical Engineering: Imaging & Visualization, 2015
http://dx.doi.org/10.1080/21681163.2015.1029080

A system for the detection of melanomas in dermoscopy images using shape and symmetry features

Margarida Ruela[a], Catarina Barata[a]*, Jorge S. Marques[a] and Jorge Rozeira[b]

[a]*Institute for Systems and Robotics, Instituto Superior Técnico, Lisboa, Portugal;* [b]*Hospital Pedro Hispano, Matosinhos, Portugal*

(*Received 24 April 2014; accepted 3 March 2015*)

Different Computer Aided Diagnosis (CAD) systems have been proposed to diagnose skin lesions in dermoscopy images. nMost of them use different types of features inspired in the ABCD rule: asymmetry, border, color and differential structures. However, it is not clear which are the most relevant types of features. In this paper we present a study on the importance of shape and symmetry features in the detection of melanomas. In order to assess the relevance of these features, a CAD system that solely uses symmetry or shape features to represent lesions was developed. In this manner, we are able to evaluate the contribution of each one of these types of features. The system was tested using the PH^2 database of annotated images from the Hospital Pedro Hispano. The CAD system achieved a sensitivity of 83%, specificity of 78% with shape features, and a sensitivity of 96% and specificity of 86%, using symmetry features. We conclude that both types of features convey discriminative information about the lesion type but symmetry plays the most important role. A comparison with color and texture features is also provided.

Keywords: melanoma; dermoscopy; shape features; symmetry features; computer aided-diagnosis

1. Introduction

1.1 Motivation

Dermoscopy is a non-invasive imaging technique that magnifies skin lesion images and allows a significant improvement of melanoma diagnosis accuracy. Other imaging modalities, such as FDG-PET and MRI, can also be used to diagnose melanomas. However, due to their characteristics, these imaging methods achieve higher diagnostic accuracies when melanomas are in late stages and have already metastasized to other organs and tissues (e.g., see Buchbender et al. 2012). On the other hand, dermoscopy can be used to diagnose melanomas in early stages, before tissue invasion. This property makes dermoscopy a powerful technique. However, the analysis of dermoscopic images involves subjective decisions and requires specific training of medical experts (Srl 2003). Several computer aided diagnosis (CAD) Systems have been developed in order to assist medical doctors in the analysis of skin lesions and in the detection of melanomas (e.g., see Ganster et al. 2001; Celebi et al. 2007).

Most of the CAD systems use a large set of features that characterize the shape, symmetry, color and texture of a lesion. These features are inspired in the ABCD rule proposed by (Nachbar et al. 1994) that computes a malignancy score for each skin lesion, based onfour criteria: its degree of (A)symmetry, (B)order irregularity, number of (C)olors and presence of (D)ermoscopic structures. CAD systems extract image features related to these four criteria in an automatic way. Typically, a few hundred features are used to represent the skin lesion taking into account symmetry, shape, color and texture (dermoscopic structures) but few attempts have been made to select the best features for each of these criteria.

This paper aims to study the influence of shape and symmetry features on the detection of melanomas. Our goal is to assess which type of features is the most discriminative. Furthermore, we also test different shape and symmetry descriptors in order to identify the most informative ones. redTo the best of our knowledge, this kind of comparative work has been scarcely explored in the dermoscopy field. The final decision (melanoma or not) is based on shape and symmetry features only. This paper extends a recent work in which color and texture features were considered and evaluated (Barata et al. 2014).

1.2 Related work

Shape and symmetry features have been considered in several CAD systems for the detection of melanomas. However, most of times they have been used in combination with color and texture-related features (e.g., Rubegni et al. 2002; Iyatomi et al. 2008). Few exceptions are the works of Claridge et al. (1992), who evaluate the performance of shape descriptors, and of Schmid-Saugeonaa et al. (2003)) and Seidenari et al. (2005); Seidenari et al. (2006), who investigated the role of symmetry. By comparison, color descriptors have been

*Corresponding author. Email: ana.c_dalgo.barata@ist.utl.pt

addressed in a larger number of works, such as (Seidenari et al. 2003; Barata et al. 2014; Celebi & Zornberg 2014).

Dermatologists assume that benign lesions usually have small dimensions and a shape similar to a circle. Thus, CAD systems must compute shape features that described these two characteristics. Some of the more popular features are the area, the perimeter and the compactness index of the lesions. These features have been widely used in different works, such as (Andreassi et al. 1999; Celebi et al. 2007). Other shape descriptors include measures of rectangularity (e.g., Iyatomi et al. 2008), ellipticity (e.g., Rubegni et al. 2002; Celebi et al. 2007) and eccentricity (e.g., Celebi et al. 2007).

Another important aspect considered by dermatologists is the border of the lesion. Therefore, it is also common to include shape features that characterize the border of the lesion, such as the fractal dimension used by Andreassi et al. (1999) and Claridge et al. (1992) and the irregularity index (see Lee et al. 2003).

The shape features mentioned above are commonly computed using a binary mask obtained by lesion segmentation. This makes the extraction of shape features highly dependent on the segmentation results. As a result, we assess the influence of segmentation inperformance of the CAD system, by comparing the classification results obtained with the optimal segmentation (performed by a dermatologist), with the ones obtained with an automatic segmentation algorithm.

The medical assessment of lesion symmetry can be performed in two different ways. Dermatologist can look for the presence of absence of shape symmetry, as well as, at the distribution of colors and textures and determine if their arrangement is symmetric or asymmetric. To mimic this analysis, CAD systems assess the symmetry of the lesion either using the binary segmentation mask, as described in Celebi et al. (2007), the color image (e.g., Seidenari et al. 2006) and/or the gray scale image (e.g., Schmid-Saugeonaa et al. 2003).

A common approach to assess shape symmetry consists in diving the binary mask according to its principal axis. Then, the mirrored image of one of the halves is overlapped with the other half. The degree of symmetry regarding the principal axis is given bycomputing the area difference between the two overlapping folds. Finally, the procedure is repeated using the second principal axis.

Color and texture information can be used to compare pixels at symmetric positions, as described in Gutkowicz-Krusin et al. (1997) and Schmid-Saugeon (2000), or to compare symmetric blocks (Seidenari et al. 2006). In the latter case, the lesion has to be divided in patches and color or texturefeatures are computed for each patch. These features are then used to compare the symmetric patches and compute a symmetry score. A different approach consists of using color or texture information to determine the direction of the symmetry axes, as proposed in Schmid-Saugeon (2000), where the authors determine the axes that maximize symmetry using symmetry maps.

In this work we investigate the performance of different shape and symmetry descriptors. Among the possible shape descriptors we selected the following five: simple shape (SS) descriptors (area, compactness, minor and major axis length and rectangularity), Hu's and Wavelets invariant moments, Žunić compactness, and Fourier descriptors (FDs). Regarding the symmetry, we evaluate the importance of shape and color symmetries. Some of the tested descriptors have been previously used in other works to describe the shape and symmetry of a lesion, namely SS descriptors, hu's moments, and shape symmetry (for more details refer to Korotkov and Garcia (2012)). Other descriptors have also been applied to dermoscopy images, but with a goal different from the one of this paper: Fourier and Wavelets (see Korotkov & Garcia 2012). To the best of our knowledge the Žunić compactness and the strategy used to assess color symmetry have not been used in the dermoscopy context.

1.3 Contributions

As aforementioned, most CAD systems use a combination of shape, color and texture features as lesion descriptors. In this article, we assess the performance of a CAD system considering shape or color symmetry features. The main contributions of this work are the following:

- Separate evaluation of shape and symmetry information;
- Identification of informative shape and color symmetry descriptors;
- Comparison between manual and automatic segmentation.

The article is organized as follows. Section 2 presents an overview of the developed system. Sections 3 and 4 present, respectively, brief descriptions on the applied shape and symmetry descriptors. Section 5 presents the experimental results alongside with their respective discussion and Section 6 presents the conclusions.

2. Computer-aided diagnosis system

This paper describes a CAD system for the detection of melanomas in dermoscopic images, based on shape and symmetry features. The proposed system comprises three stages (see Figure 1): (i) lesion segmentation, (ii) feature extraction and (iii) lesion classification.

The first block aims to separate the pigmented skin lesion from the healthy skin. Two segmentation methods are considered in this paper: (i) manual segmentation performed by an expert, considered as ground truth, and

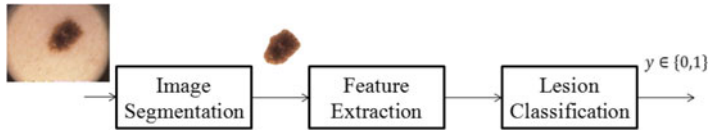

Figure 1. Block diagram of the classification system.

(ii) automatic segmentation based on an adaptive thresholding algorithm described in Barata et al. (2014). Figure 2 shows the results obtained by both approaches in two dermoscopy images. They agree on the first example but the adaptive threshold method fails to detect the white part of the lesion in the second example. This is not surprising since it is well known that automatic segmentation methods may fail to detect these kind of legions and often consider them as part of the healthy skin. A detailed account on lesion segmentation can be found in Celebi et al. (2009).

It is well known that melanomas are often associated with large lesions with irregular borders and an uneven pigment distribution. The second block extracts a set global features conveying shape and symmetry information. Each lesion is represented by a set of global features. Shape features are extracted from the lesions' binary segmentation mask whereas color symmetry features are based on the spatial distribution of colors in the lesion. Feature extraction will be further discusses in Sections 3 and 4.

A statistical classifier is then used to discriminate melanoma images from non-melanoma ones. The classifier parameters are first learned using a training set of dermoscopy images, labeled by an expert. The classifier is then applied to automatically label new images which were not used during the training phase. The classification algorithm used in this paper is the the k-nearest neighbors (k-NN) method (see Duda et al. 2001). This classification algorithm was used in several automatic systems, as stated in Korotkov & Garcia (2012). In this work, more complex algorithms were tested as well (AdaBoost and SVM) and kNN achieved similar performances to both of them. This was also noted in another work (see Barata et al. 2014), where k-NN performed as well as AdaBoost and better than SVM. Since the performances were similar and kNN is significantly easier to implement, we decided to use kNN is all the systems.

The described system is compatible with the CAD system developed in Barata et al. (2014) for the evaluation of color and texture features in the detection of melanomas. This is another reason for choosing the k-NN method since this allows a direct comparison of results with the ones obtained this paper.

3. Shape analysis

We will consider five shape descriptors which will be evaluated and compared: SS descriptor, moment invariants, wavelet moment descriptor, FD and a combination of Žunić compactness and moment invariants. All of them are computed from the binary segmentation mask $B(x, y)$ and are invariant with respect to translation and rotation.

3.1 Simple shape descriptor

The SS descriptor comprises five of the simplest shape features: area (A), compactness (C), minor (l) and major (L) axis length and rectangularity (R). The area corresponds to the number of active pixels of the binary segmentation mask. The compactness index

$$C = \frac{4\pi A}{P^2}, \tag{1}$$

characterizes the similarity between a lesion shape and a circle with the same perimeter (P). The minor and major axis lengths are obtained by approximating the lesion region by an elipse, using principal component analysis (see details in Section 4). Finally, rectangularity, is the

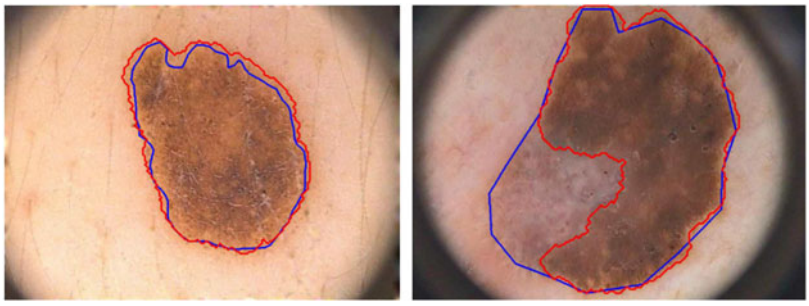

Figure 2. (Colour online) Examples of lesion segmentation: Manual Segmentation (blue) and Automatic Segmentation (red).

ratio between the area of the lesion and the area of the smallest rectangle that contains the lesion. Despite their simplicity, these features convey useful information about the lesion shape.

3.2 Moment invariants

Several moment-based descriptors have been proposed in the shape analysis literature, including Hu invariants, Zernike, Legendre, Chebyshev and wavelet moments (e.g., see Celebi & Aslandogan 2005). In this work, we consider two of these descriptors: the moment invariants proposed by (Hu 1962) and the wavelet invariant moments described in Shen & Ip (1999).

Given a binary lesion mask $B(x, y)$, the central moment of order p, q is defined by

$$\mu_{pq} = \sum_{x,y} (x - \bar{x})^p (y - \bar{y})^q B(x, y), \tag{2}$$

where $(\bar{x}, \bar{y})$ are the coordinates of the lesion center. The set of all moments provides a complete representation of the image, in the sense that there is a 1-1 map between the binary image and the set of moments, as shown in Jain (1989). The central moments are invariant to translations but they are not invariant to scaling and rotation. Invariance to scaling can be easily achieved by a suitable normalization. Invariance to rotation is however a more difficult goal. Hu proposed a set of 7 descriptors (moment invariants) that are invariant to rotation, translation and scaling (see Hu 1962; Jain 1989).

3.3 Wavelet invariant moments

Another strategy to guarantee translation, rotation and scaling invariance is by use of a wavelet shape descriptor. This descriptor comprises a set of wavelet moments which are obtained by projecting the mask $B(x, y)$ onto a wavelet basis function. This descriptor, proposed in (Shen and Ip, 1999), is able to provide both global and local information about the shape of the object.

The wavelet moments are computed as follows. Firstly, translation and scaling invariance are achieved by a change of variables

$$\mathbf{x}' = \sqrt{\frac{\alpha}{A}}(\mathbf{x} - \bar{\mathbf{x}}), \tag{3}$$

where $\mathbf{x}$ is a vector containing the coordinates (x, y) of a pixel, $\bar{\mathbf{x}}$ is a vector containing the coordinates $(\bar{x}, \bar{y})$ of the object's centroid, A is the lesion area and α is a constant. Then the binary mask $B(x,y)$ is converted to polar coordinates $B_p(r, \theta)$, the conversion being defined by

$$x = r\cos(\theta) \quad y = r\sin(\theta). \tag{4}$$

The wavelet moments are computed according to (Shen and Ip, 1999)

$$M_{m,n,q} = \int\int B(r, \theta)\psi_{m,n}(r)e^{jq\theta} r \, \mathrm{d}r \, \mathrm{d}\theta, \tag{5}$$

where $\psi_{m,n}$ is the wavelet basis function. Invariance to rotation is achieved by computing $|M_{m,n,q}|$ (see (Shen and Ip, 1999) for additional details).

3.4 Žunić compactness

Compactness is a measure of the similarity between a shape $B(x, y)$ and a circle with the same perimeter. Žunić et al. (2010) recently proposed a new compactness measure based on the first Hu moment invariant

$$C = \frac{1}{2\pi} \frac{\mu_{0,0}^2}{\mu_{2,0} + \mu_{0,2}}. \tag{6}$$

In Žunić et al. (2010) the authors also introduced a parameter β which enables the adjustment of the compactness measure to specific problems, as follows

$$C_\beta = \begin{cases} \dfrac{\mu_{0,0}^{\beta+1}}{(\beta+1)\pi^\beta \sum_{(x,y)\in B}(x^2+y^2)^\beta}, & \beta > 0 \\ \dfrac{(\beta+1)\pi^\beta \sum_{(x,y)\in B}(x^2+y^2)^\beta}{\mu_{0,0}^{\beta+1}}, & \beta \in [-1, 0]. \end{cases} \tag{7}$$

3.5 Fourier descriptors

FDs are contour-based shape descriptors that are invariant to rotation, translation and changes in scale, as defined in Zhang and Lu (2003). These descriptors are computed as follows. First, the lesion contour is sampled at N equally spaced points. These points define a complex signal

$$z(n) = x(n) + jy(n) \quad n = 0, 1, \ldots, N-1, \tag{8}$$

where $(x(n), y(n))$ are the coordinates of the $n-th$ sampled point. The finite length signal $z(n)$ can be represented by a discrete Fourier transform (DFT)

$$z(n) = \frac{1}{N}\sum_{k=0}^{N-1} c_k e^{j(2\pi/N)nk} \quad n = 0, 1, \ldots, N-1. \tag{9}$$

where c_k is the $k-th$ DFT coefficient. The DFT coefficients represent the lesion boundary. However they are not invariant to translation, rotation and scaling. Translation invariance is achieved by ignoring the DC coefficient, c_0; rotation and scaling invariance are achieved by computing

the modulus and normalizing (Jain, 1989)

$$c'k = \frac{|c_k|}{\sum_{j=1}^{N-1}|c_j|} \quad k = 1, 2, \ldots, N-1. \tag{10}$$

4. Symmetry analysis

The symmetry of a skin lesion is an important cue to asses its degree of malignancy. Symmetric lesions with respect to two axis tend to be benign while highly asymmetric lesions produced by an abnormal increase of melanocytic cells may often be melanomas. Two symmetry types are considered in this paper: (i) shape symmetry, computed from the binary segmentation mask and (ii) color symmetry, computed from the spatial distribution of color within the lesion. In both cases, pixels associated with the healthy skin are discarded.

4.1 Shape symmetry

In this paper, we consider two sets of shape symmetry features. The first is obtained by dividing the image into halves, along the principal axes, and by folding one half of the lesion over the mirror image of the other half. Figure 3 shows an example of this procedure. The degree of symmetry (s) is defined by

$$s = \frac{2A_{\text{Intersection}}}{A_{\text{Lesion}}}, \tag{11}$$

where $A_{\text{Intersection}}$ corresponds to the area of intersection between the two halves of the lesion (in pixels) and A_{lesion} is the total area of the lesion. The $A_{\text{Intersection}}$ is represented in red in Figure 3.

The second symmetry measure is obtained by dividing the lesion into an even number of slices with a common vertex at lesion centroid. Each slice is overlapped with the mirrored image of its opposite slice and the degree of symmetry is given by the fraction between twice the number of overlapped pixels and the sum of the areas of the two slices (in pixels). Figure 4 exemplifies the superposition between the slices. The degree of symmetry (s) is given by

$$s = \frac{2A_{ij}}{A_i + A_j}, \tag{12}$$

where A_{ij} corresponds to the area of intersection between the two slices (in pixels) and A_i, A_j are the areas of the opposite slices i and j. In Figure 4 A_{ij} corresponds to the red region and A_i, A_j correspond to the blue and yellow regions.

4.2 Color symmetry

Color symmetry analysis is performed by assessing the overall color similarity between symmetric blocks. This process is divided into three main stages: (i) rotated grid computation, (ii) local feature extraction and (iii) calculation of distortion measures.

4.2.1 Grid computation

First two symmetry axes are determined by using principal component analysis (Jolliffe, 2002). Let **R** be the covariance

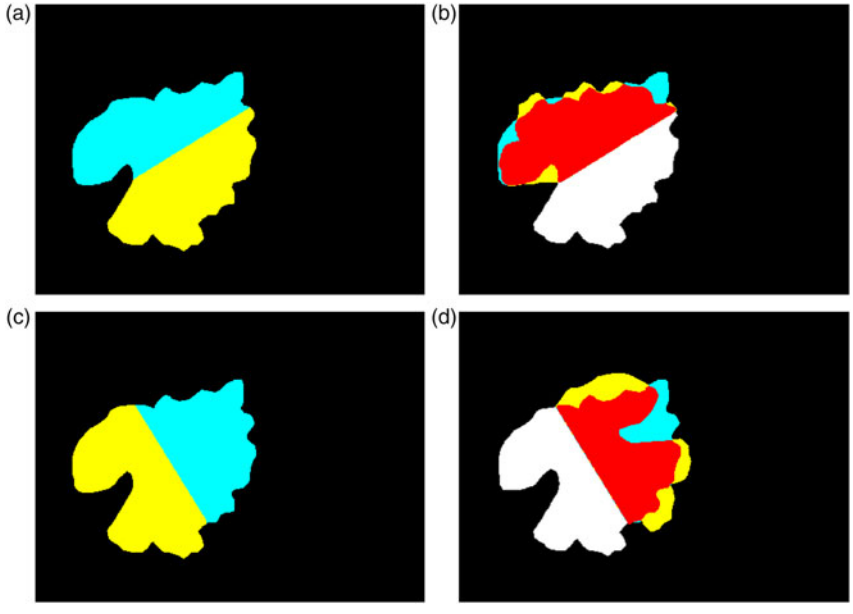

Figure 3. (Colour online) Analysis of the symmetry regarding the axes of the lesion: (a) and (c) lesion divided into halves according to the principal axes of the image, (b) and (d) show the overlap (red) between one of the halves of the lesion (blue) and the mirrored image of the other half (yellow).

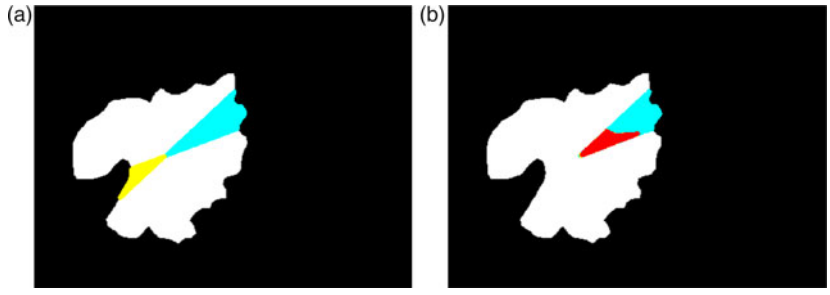

Figure 4. (Colour online) Analysis of the symmetry between opposite slices: (a) two opposite slices of the lesion and (b) overlap (red) between one of the slices (blue) and the mirrored image of its opposite slice (yellow).

matrix of the binary segmentation mask $B(x, y)$ with N active pixels

$$\mathbf{R} = \frac{1}{N} \sum_{\mathbf{x}:B(\mathbf{x})=1} (\mathbf{x} - \bar{\mathbf{x}})(\mathbf{x} - \bar{\mathbf{x}})^T, \tag{13}$$

where $\mathbf{x} = (x, y)$ is a vector containing the coordinates of a lesion pixel, N is the number of lesion pixels and $\bar{\mathbf{x}}$ is the mass center of the lesion mask. Let λ_i and $\mathbf{v}_i$, $i \in \{1, 2\}$, be the eigenvalues and eigenvectors of $\mathbf{R}$, respectively. The nodes of the regular grid are defined as follows

$$\mathbf{x}_{jk} = j\Delta_1\mathbf{v}_1 + k\Delta_2\mathbf{v}_2 + \bar{\mathbf{x}}, \quad j, k \in \mathbb{Z}, \tag{14}$$

where

$$\Delta_i = c\sqrt{\lambda_i}, \quad i \in \{1, 2\}, \tag{15}$$

and c is a constant which defines the distance between the grid nodes. Figure 5 shows (a) an example of the principal components of a lesion and (b) the regular grid defined over the same lesion.

4.2.2 *Local features*

A set of color features are extracted from valid grid blocks (see Figure 5). A block is considered as valid if at least 25% of its area overlaps the lesion. Three color descriptors computed in four color spaces were used to represent the blocks. The set of color descriptors includes the uni-dimensional color histogram (UCH), the mean color vector (MCV) and the generalized color moments (GCM), whereas the set of color spaces includes the RGB, HSV, L*a*b* and Opponent spaces. These color spaces were chosen based on the results of a previous study by (Barata et al. 2014). The descriptors used to characterize each cell are the following:

- Mean Color Vector (MCV) - is a 3D vector with the mean color components within the block.
- Uni-dimensional Color Histogram (UCH) - The range of values of each color channel is divided into disjoint intervals (bins). The histogram value associated to each bin is proportional to the number of pixels that fall into that bin.
- Generalized Color Moments (GCM) - These moments were proposed by Mindru et al. (2004) and provide information about the color and shape of the image. A GCM of order $p + q$ and degree $a + b + c$ is defined by

$$M_{pq}^{abc} = \sum_{(x,y)\in\text{Block}} x^p.y^q.[I_1(x, y)]^a .[I_2(x, y)]^b.[I_3(x, y)]^c, \tag{16}$$

where I_i corresponds to the intensity of the ith color channel, $i \in \{1, 2, 3\}$. Since the moments of smaller order and degree are more robust against noise, only moments of order $p + q \leq 1$ and degree $a + b + c \leq 2$ are used to describethe lesion.

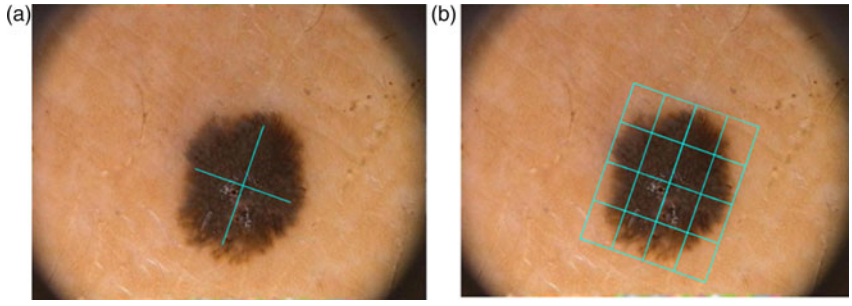

Figure 5. Regular grid of nodes: (a) principal axis; (b) grid nodes.

4.2.3 Calculation of distortion measures

The previous section describes each block by a feature vector. Now, we need to compare the features of symmetric blocks leading to a set of block-based distortion measures. These measures cannot be used as features since their number depends on the number of blocks, thus it is lesion dependent. To overcome this difficulty the following strategy was adopted.

Lets define S_k as the sets of all pairs of symmetric blocks (i,j) according to the $k = 1, 2$ principal axes. The first step consists of computing a distance measure between symmetric blocks for each set S_k. The adopted measure is the Euclidean distance

$$d_{ij} = \left\|\mathbf{x}_i - \mathbf{x}_j\right\|, \tag{17}$$

where $\mathbf{x}_i$, $\mathbf{x}_j$ are the feature vectors associated with the pair (i,j) of symmetric blocks.

Then, statistical measures are computed to characterize each of the sets. The measures are: mean μ_k, standard deviation σ_k, maximum M_k, and minimum m_k. Each of these measures is computed as follows

$$\mu_k = \frac{1}{\#S_k} \sum_{(i,j)\in S_k} d_{ij}, \tag{18}$$

$$\sigma_k = \frac{1}{\#S_k} \sum_{(i,j)\in S_k} (d_{ij} - \mu_k)^2, \tag{19}$$

$$M_k = \max\{d_{ij} : (i,j) \in S_k\}. \tag{20}$$

$$m_k = \min\{d_{ij} : (i,j) \in S_k\}, \tag{21}$$

Finally it is possible to obtain an image feature vector as follows:

$$\mathbf{d} = [\mu_1, \sigma_1, M_1, m_1, \mu_2, \sigma_2, M_2, m_2] \tag{22}$$

5. Experimental results and discussion

5.1 Dataset and performance metrics

Experimental tests were performed using the PH^2 (Mendonça et al. 2013) database of dermoscopy images from Hospital Pedro Hispano, Portugal. However, we had to exclude the images for which the lesions intersect the boundary, so that we could perform border and symmetry analysis. The final dataset comprises 169 lesions: 24 melanomas and 145 non melanomas. The images were acquired by a dermatologist during routine clinical examinations using a dermatoscope with a magnification of 20×. Each lesion has an associated clinical diagnosis, performed by an expert.

Artifacts (hair, reflection) were removed during a preprocessment stage. The resulting gaps were filled by using an in painting algorithm, as described in Barata et al. (2012).

The performance of the system was assessed by computing its sensitivity (SE) and specificity (SP), using 10-fold stratified cross validation. These metrics are combined into a performance index (PI) that assigns a greater weight to SE than to SP since the misdiagnosis of melanomas has more severe consequences. The adopted PI is the following:

$$\mathrm{PI} = 1 - \frac{3}{5}\mathrm{SE} - \frac{2}{5}\mathrm{SP}. \tag{23}$$

5.2 Feature selection

The performance of the k-NN classifier degrades in high dimensional feature spaces. Therefore, a feature selection method was used to reduce the number of shape and symmetry features.

Three different approaches are often used (see Guyon & Elisseeff 2003): filters, wrappers and embedded methods. In this paper, we have selected the subset of features using a filter approach and, as in Shen and Ip (1999), we have applied the following between-to within-class variance ratio to perform feature selection

$$S = \frac{(\sigma_1 + \sigma_2)}{|\mu_1 - \mu_2|}, \tag{24}$$

(μ_i, σ_i) are the mean and intra-class standard deviation of class i, $i \in \{1, 2\}$. This measure is similar to the square root of the between-to within-class scatter, used in the Fisher Linear Discriminant (Duda et al. (2001). Then, S is sorted in ascending order and the features that correspond to the first N_{selected} values of S are selected.

5.3 Optimization of parameters

In order to determine which are the best system configurations, different descriptors (see Table 1) and several parameters were tested.

In the case of shape symmetry the parameter to be tuned was the number of slices, S, defined in the symmetry-related shape (SRS) descriptor ($S \in \{4, 8, 16\}$). Regarding the color symmetry analysis, for all three descriptors the tuned parameters were the color space (RGB, HSV, L*a*b and Opponent) and constant c ($c \in \{0.75, 1, 1.25, 1.5\}$), see (15). Furthermore, for both the UCH and the MCV we also tuned the color channel, to determine whether to use a single channel or all three channels. Finally, we also optimized the number of bins, b, of the UCH ($b \in \{5, 15, \ldots, 45\}$).

Concerning the shape descriptors, we have tuned the number of equally spaced points, N, sampled from the border of the lesion in the FD. Regarding the Žunić's

Table 1. Descriptors' acronyms.

Descriptor	Acronym
Simple shape descriptor	SS
Moment invariants	MI
Wavelet moment descriptor	WD
Fourier descriptor	FD
Žunić's compactness	ZC
Symmetry-related shape descriptor	SRS
Uni-dimensional color histogram	UCH
Generalized color moments	GCM
Mean color vector	MCV

Compactness descriptor, each entry of the feature vector corresponds to the Žunić's compactness measure computed using a given value of β. In this study, we evaluated ZC using three different subsets of β values: $B_1 = \{-0.9, -0.8, \ldots, -0.1\})$, $B_2 = \{0.1, 0.2, \ldots, 1\}$ and $B_3 = 1, 2, \ldots, 5$.

Regarding k-NN, we have chosen to use the Euclidean distance. The number of nearest neighbors was selected in the interval ($k \in \{5, 7, \ldots, 35\}$). We have also changed the number of features, $\#SF \in \{2, 3, 4, 5, 10, 20, 50, 75, 100\}$), in the cases where feature selection improves the performance, see 5.2.

Since k-NN is strongly affected by class imbalance the feature vectors related to the melanomas of the training set were oversampled until both classes reached the same number of examples. Then, we added Gaussian noise ($wN(0, \sigma_n), \sigma_n = 0.001$) to each repeated feature vector. Furthermore, all feature vectors $\mathbf{f}$ were normalized as follows:

$$\tilde{\mathbf{f}}_\mathbf{i} = \frac{\mathbf{f}_\mathbf{i} - \mu_i}{\sigma_i}, \tag{25}$$

where $\mathbf{f}_\mathbf{i}$ is the i-th element of $\mathbf{f}$ and μ_i, σ_i are, respectively, the mean and standard deviation of $\mathbf{f}_\mathbf{i}$.

5.4 *Shape analysis*

In this section we analyze the performance of the CAD system using shape features. Table 2 shows the best performances obtained for the main configurations of the system, using manually segmented lesions. The descriptors are divided in two classes: scale invariant and scale dependent descriptors. The MI, WD and FD descriptors were considered in both classes. The best single result, SE = 83% and SP = 78%, was obtained using the scale dependent WD. Nonetheless, the scale invariant version of the WD descriptor also performs well.

Table 2. Melanoma detection using shape descriptors (manual segmentation).

	Scale invariant			Scale dependent		
Descriptor	SE	SP	PI	SE	SP	PI
SS				92%	60%	0.208
MI	75%	58%	0.318	88%	63%	0.220
WD	**79%**	**79%**	**0.210**	**83%**	**78%**	**0.190**
ZC	83%	56%	0.238			
FD	79%	56%	0.302	92%	66%	0.184

Note: Bold highlights are the best results.

Table 3. Melanoma detection using shape descriptors (automatic segmentation).

	Scale invariant			Scale dependent		
Descriptor	SE	SP	PI	SE	SP	PI
SS				88%	73%	0.180
MI	79%	70%	0.246	92%	68%	0.176
WD	**88%**	**83%**	**0.140**	**92%**	**72%**	**0.160**
ZC	67%	55%	0.378			
FD	96%	60%	0.184	92%	72%	0.160

Note: Bold highlights are the best results.

Table 3 illustrates the performance of system when the manual segmentation performed by a medical expert is replaced by an automatic segmentation. The classification results are better for most of the descriptors, excluding ZC. This behavior can be explained by comparing the outputs of the two segmentation methods. Manual segmentations are usually looser than automatic ones, since dermatologists usually look for outmost pigmented pixels and start their segmentation from that point (as was pointed out in Emre Celebi et al. (2007)). This does not happen in an adaptive thresholding algorithm, as the one used in this paper. Furthermore, segmentation errors like missing white-regions, alter the size and shape of the lesion, making them look less circular (recall the right image of Figure 2). These segmentation errors may help the classifier to detect melanomas better. Another interesting aspect is that the manual borders are usually smoother than the ones obtained automatically, which can improve the performance of the border descriptors like FD. The best performance is achieved with the WD descriptors, but in this case using the scale invariant ones (SE = 88% and SP = 83%). These tests show that good classification results are obtained using shape information only.

5.5 *Symmetry analysis*

In this section, we present and analyze the performance of the system using symmetry features.

Table 4 shows the best results achieved by the system for each of the symmetry descriptors. The best result, SE = 96% and SP = 83%, was achieved using the MCV descriptor and all three channels of the HSV color space, which proved to be the best color space. UCH and GCM also achieved a good performance, while SRS performed poorly. The best results of SRS were obtained using the second symmetry measure (see (13)). This result indicates

Table 4. Melanoma detection using symmetry descriptors (manual segmentation).

Descriptor	Channel	SE	SP	PI
SRS	–	67%	59%	0.362
MCV	H + S + V	**96%**	**83%**	**0.092**
UCH	H	100%	76%	0.096
GCM	H + S + V	92%	85%	0.108

Note: Bold highlights are the best results.

that the analysis of lesion symmetry benefits from including other information besides the binary segmentation mask.

Table 5 shows the performance of symmetry descriptors when applied to automatically segmented images. The performance of the SRS descriptor improves. Since this descriptors consists of comparing symmetric slices of the binary mask, it is possible to justify the performance improvement with segmentation errors as the one of the right image of Figure 2. The performance of the color-based descriptors is less affected, which suggests that these descriptors are relatively independent of the segmentation method used.

5.6 *Shape, asymmetry, color and texture*

Most CAD systems for melanoma detection are based on the ABCD rule of dermoscopy proposed by Nachbar et al. (1994). According to this rule, the classification of melanomas depends on four parameters: asymmetry (A), border (B), color (C) and differential structures (D). The contribution of each one of theses features to CAD systems is not usually studied. In the ABCD rule of dermoscopy each parameter is assigned a given weight, however, CAD systems may require a different weight distribution.

In this article the role of shape and symmetry features was individually assessed by the development of CAD systems whose classification depended on only one of these parameters. We can extend this study with the results described in Barata et al. (2014) which considered the detection of melanomas using color and texture features. The best performance achieved by each type of descriptors is shown in Table 6. This comparison is possible because we are using the same dataset, excluding the images for which the lesions were larger than the field of the image.

Table 5. Melanoma detection using symmetry descriptors (automatic segmentation).

Descriptor	Channel	SE	SP	PI
SRS	–	79%	63%	0.274
MCV	H + S + V	92%	77%	0.140
UCH	H	**100%**	**75%**	**0.100**
GCM	H + S + V	96%	77%	0.116

Note: Bold highlights are the best results.

Table 6. Melanoma detection using four different types of descriptors.

Descriptors	SE	SP	PI
Symmetry	**96%**	**83%**	**0.092**
Shape	83%	78%	0.190
Color	93%	85%	0.104
Texture	96%	59%	0.188

Note: Color and texture results are the ones obtained by (Barata et al. 2014). Bold highlights are the best results.

These results show that, even though all four classes of features are important, color and color symmetry features play the most important role since they lead to the correct classification of most lesions by achieving performances of SE = 93%, mboxSP = 85% and SE = 96%, SP = 83%.

6. Conclusions and future work

This paper addresses the role of symmetry and shape descriptors in the detection of melanomas in dermoscopy images. Several symmetry and shape descriptors were separately analyzed in order to assess their individual contributions. We also analyzed the influence of the segmentation methods (manual vs. automatic) in the performance of the system.

The best results were obtained by comparing the color of symmetric patches (squares), each patch being represented by the average color in the HSV color space. This procedure achieved promising scores (SE = 96%, SP = 83%) in the detection of melanomas on the PH^2 public domain database. Very good results were also achieved by the analysis of the lesion shape. Several descriptors were considered and the best scores were obtained using the wavelet moments (SE = 83%, SP78%).

A comparison with the color and texture features using the same data set of dermoscopic images, allows us to conclude that the most discriminative features are the ones related to color symmetry, closely followed by color features.

These results can be easily compared with the ones provided by other authors since the PH^2 database is a public one. The next step concerns the fusion of the different types of features. This is done in the ABCD rule through a weighted sum of individual scores obtained for each of the four feature types (asymmetry, border (shape), color and differential structures (texture)). This can also be done in the context of machine learning algorithms by combining the output of separate classifiers. This can be done is several ways. This will probably lead to a further increase of performance and robustness.

Acknowledgements

The authors would like to thank the Service of Dermatology of Hospital Pedro Hispano, as well as Prof. Teresa Mendonça and

Pedro Ferreira, University of Porto, for providing the database of dermoscopic images, PH^2, with clinical anotations. A special thanks to the anonymous reviewers, who provided insightful comments that improved the quality of the paper.

Conflict of interest disclosure statement

No potential conflict of interest was reported by the authors.

Funding

This work was supported by Fundação para a Ciência e Tecnologia in the scope of the [grant number SFRH/BD/84658/2012] and projects [PTDC/SAU-BEB/103471/2008] and [PEst-OE/EEI/LA0009/2011].

References

Andreassi L, Perotti R, Rubegni P, Burroni M, Cevenini G, Biagioli M, Taddeucci P, Dell'Eva G, Barbini P. 1999. Digital dermoscopy analysis for the differentiation of atypical nevi and early melanoma. Arch Dermatol. 135(12):1459–1465. doi:10.1001/archderm.135.12.1459.

Barata C, Figueiredo MAT, Celebi ME, Marques JS. 2014. Color identification in dermoscopy images using gaussian mixture models. 2014 IEEE International Conference on Acoustics, Speech and Signal Processing (ICASSP). Florence, Italy: IEEE; p. 3611–3615.

Barata C, Marques JS, Rozeira J. 2012. A system for the detection of pigment network in dermoscopy images using directional filters. IEEE Trans Biomed Eng. 59(10):2744–2754. doi:10.1109/TBME.2012.2209423.

Barata C, Ruela M, Francisco M, Mendonça T, Marques J. 2014. Two systems for the detection of melanomas in dermoscopy images using texture and color features. IEEE Syst J. 8(3):965–979. doi:10.1109/JSYST.2013.2271540.

Buchbender C, Heusner TA, Lauenstein TC, Bockisch A, Antoch G. 2012. Oncologic pet/mri, part 2: bone tumors, soft-tissue tumors, melanoma, and lymphoma. J Nucl Med. 53(8):1244–1252. doi:10.2967/jnumed.112.109306.

Celebi ME, Aslandogan YA. 2005. A comparative study of three moment-based shape descriptors. In: International Conference on Information Technology: Coding and Computing (ITCC). vol. 1. Las Vegas, NV: IEEE; p. 788–793.

Celebi ME, Zornberg A. 2014. Automated quantification of clinically significant colors in dermoscopy images and its application to skin lesion classification. IEEE Syst J. 8(3):980–984. doi:10.1109/JSYST.2014.2313671.

Celebi ME, Iyatomi H, Schaefer G, Stoecker W. 2009. Lesion border detection in dermoscopy images. Comput Med Imaging Graphics. 33(2):148–153. doi:10.1016/j.compmedimag.2008.11.002.

Celebi ME, Kingravi HA, Uddin B, Iyatomi H, Aslandogan YA, Stoecker WV, Moss RH. 2007. A methodological approach to the classification of dermoscopy images. Comput Med Imaging Graphics. 31(6):362–373. doi:10.1016/j.compmedimag.2007.01.003.

Claridge E, Hall PN, Keefe M, Allen J. 1992. Shape analysis for classification of malignant melanoma. J Biomed Eng. 14(3):229–234. doi:10.1016/0141-5425(92)90057-R.

Emre Celebi ME, Alp Aslandogan YA, Stoecker WV, Iyatomi H, Oka H, Chen X. 2007. Unsupervised border detection in dermoscopy images. Skin Res Technol. 13(4):454–462. doi:10.1111/j.1600-0846.2007.00251.x.

Duda RO, Hart PE, Stork DG. 2001. Pattern classification. Wiley. Pattern Classification and Scene Analysis: Pattern Classification.

Ganster H, Pinz A, Rohrer R, Wildling E, Blinder M, H K. 2001. Automated melanoma recognition. IEEE Trans Biomed Eng. 20(3):233–239.

Gutkowicz-Krusin D, Elbaum M, Szwaykowski P, Kopf AW. 1997. Can early malignant melanoma be differentiated from atypical melanocytic nevus by *in vivo* techniques? Skin Res Technol. 3(1):15–22. doi:10.1111/j.1600-0846.1997.tb00154.x.

Guyon I, Elisseeff A. 2003. An introduction to variable and feature selection. J Mach Learn Res. 3:1157–1182.

Hu M-K. 1962. Visual pattern recognition by moment invariants. IRE Trans Inf Theory. 8(2):179–187. doi:10.1109/TIT.1962.1057692.

Iyatomi H, Oka H, Celebi ME, Hashimoto M, Hagiwara M, Tanaka M, Ogawa K. 2008. An improved internet-based melanoma screening system with dermatologist-like tumor area extraction algorithm. Comput Med Imaging Graphics. 32(7):566–579. doi:10.1016/j.compmedimag.2008.06.005.

Jain AK. 1989. Fundamentals of digital image processing. vol. 3. Englewood Cliffs, NJ: Prentice-Hall.

Jolliffe IT. 2002. Principal component analysis. 2nd, 2nd ed. Springer.

Korotkov K, Garcia R. 2012. Computerized analysis of pigmented skin lesions: a review. Artif Intell Med. 56(2):69–90. doi:10.1016/j.artmed.2012.08.002.

Lee TK, McLean DI, Stella Atkins MS. 2003. Irregularity index: A new border irregularity measure for cutaneous melanocytic lesions. Med Image Anal. 7(1):47–64. doi:10.1016/S1361-8415(02)00090-7.

Mendonça T, Ferreira PM, Marques J, Marcal AR, Rozeira J. 2013. Ph 2-a dermoscopic image database for research and benchmarking. In: 35th Annual International Conference of the IEEE Engineering in Medicine and Biology Society (EMBC). Osaka, Japan: IEEE; p. 5437–5440.

Mindru F, Tuytelaars T, Van Gool L, Moons T. 2004. Moment invariants for recognition under changing viewpoint and illumination. Comput Vision Imaging Understanding. 94(1–3):3–27.

Nachbar F, Stolz W, Merkle T, Cognetta AB, Vogt T, Landthaler M, Bilek P, Braun-Falco O, Plewig G. 1994. The abcd rule of dermatoscopy. J Am Acad Dermatol. 30(4):551–559. doi:10.1016/S0190-9622(94)70061-3.

Rubegni P, Cevenini G, Burroni M, Perotti R, Dell'Eva G, Sbano P, Miracco C, Luzi P, Tosi P, Barbini P, Andreassi L. 2002. Automated diagnosis of pigmented skin lesions. Int J Cancer. 101(6):576–580. doi:10.1002/ijc.10620.

Schmid-Saugeon P. 2000. Symmetry axis computation for almost-symmetrical and asymmetrical objects: application to pigmented skin lesions. Med Image Anal. 4(3):269–282. doi:10.1016/S1361-8415(00)00019-0.

Schmid-Saugeona P, Guillodb J, Thirana JP. 2003. Towards a computer-aided diagnosis system for pigmented skin lesions. Comput Med Imaging Graphics. 27(1):65–78. doi:10.1016/S0895-6111(02)00048-4.

Seidenari S, Pellacani G, Grana C. 2003. Computer description of colours in dermoscopic melanocytic lesion images reproducing clinical assessment. Br J Dermatol. 149(3):523–529. doi:10.1046/j.1365-2133.2003.05496.x.

Seidenari S, Pellacani G, Grana C. 2005. Pigment distribution in melanocytic lesion images: a digital parameter to be employed for computer-aided diagnosis. Skin Res Technol. 11(4):236–241. doi:10.1111/j.0909-725X.2005.00123.x.

Seidenari S, Pellacani G, Grana C. 2006. Asymmetry in dermoscopic melanocytic lesion images: a computer description based on colour distribution. Acta Derm Venereol. 86(2):123–128.

Shen D, Ip HHS. 1999. Discriminative wavelet shape descriptors for recognition of 2-D patterns. Pattern Recogn. 32(2): 151–165. doi:10.1016/S0031-3203(98)00137-X.

Srl DM. 2003. Dermoscopy tutorial. Available from: http://dermoscopy.org/atlas/base.htm

Zhang D, Lu G. 2003. A comparative study of curvature scale space and fourier descriptors for shape-based image retrieval. J Visual Commun Image Represent. 14(1):39–57. doi:10.1016/S1047-3203(03)00003-8.

Žunić J, Hirota K, Rosin PL. 2010. A hu moment invariant as a shape circularity measure. Pattern. 43(1):47–57.